

Single-Atom Catalysis

Rational Fabrication of Low-Coordinate Single-Atom Ni Electrocatalysts by MOFs for Highly Selective CO₂ Reduction

Yan Zhang, Long Jiao, Weijie Yang, Chenfan Xie, and Hai-Long Jiang*

Abstract: Single-atom catalysts (SACs) have attracted tremendous interests due to their ultrahigh activity and selectivity. However, the rational control over coordination microenvironment of SACs remains a grand challenge. Herein, a post-synthetic metal substitution (PSMS) strategy has been developed to fabricate single-atom Ni catalysts with different N coordination numbers (denoted Ni-N_x-C) on pre-designed N-doped carbon derived from metal-organic frameworks. When served for CO₂ electroreduction, the obtained Ni-N₃-C catalyst achieves CO Faradaic efficiency (FE) up to 95.6%, much superior to that of Ni-N_x-C. Theoretical calculations reveal that the lower Ni coordination number in Ni-N₃-C can significantly enhance COOH* formation, thereby accelerating CO₂ reduction. In addition, Ni-N₃-C shows excellent performance in Zn-CO₂ battery with ultrahigh CO FE and excellent stability. This work opens up a new and general avenue to coordination microenvironment modulation (MEM) of SACs for CO₂ utilization.

Single-atom catalysts (SACs) with maximized utilization of metal atoms have captured widespread interest in heterogeneous catalysis.^[1] Given that single metal atoms are stabilized by the supports based on coordination interaction, the catalytic performance of SACs is highly sensitive to their local coordination environment from the viewpoint of coordination chemistry.^[1c,2] On account of this, great efforts have been devoted to the coordination environment regulation of SACs.^[1c,2] The coordination number of SACs, an important parameter of coordination microenvironment modulation (MEM), would greatly influence the electronic and geometric structure of metal centers in SACs, playing significant roles in catalytic activity and selectivity.^[2c,3] Specifically, in single metal atoms incorporated N-doped carbon materials (M₁-N-C), the number variation of coordi-


How to cite: *Angew. Chem. Int. Ed.* **2021**, *60*, 7607–7611
 International Edition: doi.org/10.1002/anie.202016219
 German Edition: doi.org/10.1002/ange.202016219

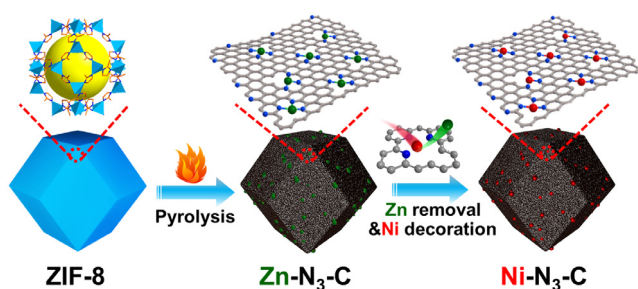
nated N atoms in SACs can induce differentiated local electronic densities of central metal atoms, which greatly affects the adsorption of reaction intermediates and modulates the catalytic activity of SACs.^[4] Although significant progress has been achieved in the construction of SACs, there is lack of effective strategy to precisely regulate coordination number without disturbing the single-atom dispersion of metal centers.^[2c,3a,d,5]

Metal-organic frameworks (MOFs),^[6] as a class of crystalline porous materials featuring tailorable composition and structure, have demonstrated particular advantages on the accurate construction of efficient catalysts.^[7] Moreover, MOFs have been recognized to be one of the most promising candidates toward precise regulation on the coordination environment of SACs.^[4,8] While great efforts have been devoted, the currently adopted strategies to the modulation of coordination number are almost limited to the one-step pyrolysis of targeted metal-doped MOF precursors, where the higher temperature leads to lower N coordination number.^[4c,5a] However, the doped metal species possibly disturbs the MOF formation. Accordingly, the synthesis of metal doped MOF must be modified according to doped metal species.^[4a,c,8c] Meanwhile, given the synchronous MOF carbonization and single atom formation, complex synthetic parameters, such as pyrolysis temperature, metal loading, etc., interplay each other in the one-step pyrolysis, seriously restricting the flexibility and universality of this strategy.^[4a,c,8c] On account of the dilemma above, the development of more general approaches is highly desired to achieve the accurate control over coordination environment in MOF-based SACs. The decoupling of MOF carbonization and single atom decoration, which can avert complex variates in the previous one-step pyrolysis method, might be a promising and easy-to-handle solution to coordination microenvironment modulation of SACs.

Herein, a facile post-synthetic metal substitution (PSMS) strategy has been developed to achieve controlled synthesis of single-atom Ni catalyst with low coordination number on a pre-designed N-doped carbon support derived from a Zn-based MOF (Scheme 1). During the pyrolysis of the Zn-MOF at 900 °C, the Zn nanoparticles (NPs), once formed, can vaporize readily due to their low boiling point and the N-doped carbon loaded with abundant Zn-N₃ sites (Zn-N₃-C) can be obtained. Taking advantage of the fragile Zn-N coordination bonds in acidic media, the single Zn atoms from Zn-N₃-C can be easily removed, leaving N-doped carbon (N-C) with abundant Zn vacancies surrounded by 3 N atoms. Upon refilling Ni atoms into Zn vacancies, the Ni-N₃-C, with single Ni atoms coordinated by 3 N atoms on the N-doped carbon, is elaborately fabricated. The Ni-N₃-C catalyst

[*] Y. Zhang, Dr. L. Jiao, C. Xie, Prof. Dr. H.-L. Jiang
 Hefei National Laboratory for Physical Sciences at the Microscale
 CAS Key Laboratory of Soft Matter Chemistry, Department of
 Chemistry
 University of Science and Technology of China
 Hefei, Anhui 230026 (P. R. China)
 E-mail: jianglab@ustc.edu.cn
 Homepage: <http://staff.ustc.edu.cn/~jianglab/>
 Dr. W. Yang
 Department of Power Engineering
 School of Energy, Power and Mechanical Engineering
 North China Electric Power University
 Baoding (P. R. China)

 Supporting information and the ORCID identification number(s) for the author(s) of this article can be found under:
<https://doi.org/10.1002/anie.202016219>



Scheme 1. Fabrication of low-coordination single-atom Ni electrocatalysts via a PSMS strategy.

presents an ultrahigh CO Faradic efficiency (FE) up to 95.6% with a turnover frequency (TOF) of 1425 h^{-1} at -0.65 V in the electrocatalytic CO_2 reduction reaction (CO_2RR), much better than that of pure N-C and $\text{Ni-N}_4\text{-C}$ involving Ni-N_4 sites. Theoretical calculations manifest that the low-coordinated Ni atoms in $\text{Ni-N}_3\text{-C}$ greatly facilitate the formation of COOH^* intermediate, thereby accelerating CO_2 reduction. More importantly, as a cathode in Zn- CO_2 battery, the $\text{Ni-N}_3\text{-C}$ exhibits excellent CO selectivity (over 90%) in the discharge process with excellent stability, paving the way to the direct utilization of SACs in energy conversion systems.

The Zn-MOF, named ZIF-8 or MAF-4,^[9] in a dodecahedral morphology with a size of $\approx 200 \text{ nm}$, presents a large surface area ($1203 \text{ m}^2\text{g}^{-1}$) (Figure 1a and S1, S2). Upon pyrolysis at 900°C , the obtained $\text{Zn-N}_3\text{-C}$ with high Zn loading of 6.64 wt% shows well retained morphology as the parent ZIF-8 (Figure 1b and c). No obvious Zn or ZnO nanoparticle is observable, indicating the possible atomic dispersion of Zn species on the carbon skeleton of $\text{Zn-N}_3\text{-C}$ (Figure 1c and S3). X-ray photoelectron spectroscopy (XPS) indicates the existence of Zn-N species in $\text{Zn-N}_3\text{-C}$ without metallic Zn (Figure S4). After the removal of Zn atoms in $\text{Zn-N}_3\text{-C}$ via HCl etching, followed by refilling extrinsic Ni atoms, the $\text{Ni-N}_3\text{-C}$ catalyst with 0.85 wt% Ni loading can be obtained. Both SEM and TEM results show that the particle

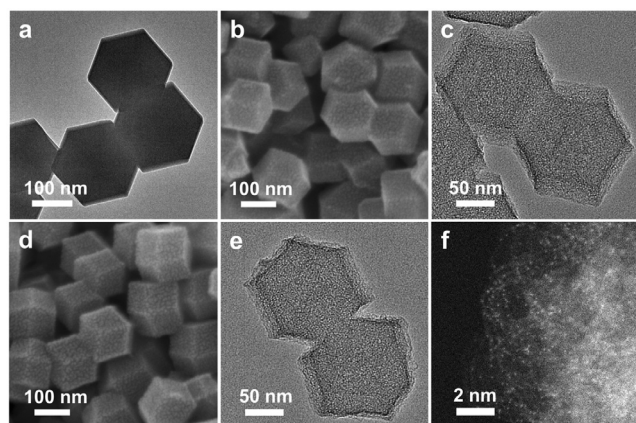


Figure 1. a) Transmission electron microscopy (TEM) image of ZIF-8, b) scanning electronic microscopy (SEM) and c) TEM images of $\text{Zn-N}_3\text{-C}$. d) SEM and e) TEM images of $\text{Ni-N}_3\text{-C}$. f) The aberration-corrected HAADF-STEM image of $\text{Ni-N}_3\text{-C}$.

size and polyhedral morphology of $\text{Ni-N}_3\text{-C}$ are almost identical to $\text{Zn-N}_3\text{-C}$ (Figure 1d and e). No metallic Ni can be identified in the TEM image of $\text{Ni-N}_3\text{-C}$, implying the possible atomic dispersion of Ni species (Figure 1e). Nitrogen sorption measurements reveal a high surface area ($821 \text{ m}^2\text{g}^{-1}$) of $\text{Ni-N}_3\text{-C}$ with similar pore size to that of $\text{Zn-N}_3\text{-C}$, manifesting the retained pore structure after the PSMS process (Figure S5).

Powder X-ray diffraction (XRD) pattern of $\text{Ni-N}_3\text{-C}$ presents two broad peaks corresponding to the (002) and (101) planes of carbon and no Ni-containing crystalline phases can be observed (Figure S6), in accordance with the above TEM results. Raman spectrum of $\text{Ni-N}_3\text{-C}$ shows a low intensity ratio of D band to G band, which is similar to $\text{Zn-N}_3\text{-C}$, indicating the high graphitization degree of $\text{Ni-N}_3\text{-C}$ (Figure S7). In addition to the characterizations on the microstructure, the chemical composition and electronic state of $\text{Ni-N}_3\text{-C}$ have been further investigated by X-ray photoelectron spectroscopy (XPS). The $\text{Ni}2\text{p}$ spectrum of $\text{Ni-N}_3\text{-C}$ indicates the Ni oxidation state locating between Ni^0 (853.0 eV) and Ni^{2+} (855.7 eV), suggesting the existence of partially oxidized Ni species (Figure S8).^[10] The N 1s spectrum can be fitted into five typical peaks corresponding to pyridinic N (398.3 eV), metal-N species (399.1 eV), pyrrolic N (400.2 eV), graphitic N (401.2 eV) and oxidized N (402.9 eV), respectively (Figure 2a).^[10] The presence of oxidized Ni and metal-N species in $\text{Ni-N}_3\text{-C}$ supports the atomic dispersion of Ni in the form of Ni-N coordination (Figure 2a and S8). Furthermore, the bright dots in the aberration-corrected high-angle annular dark-field scanning transmission electron microscopy (HAADF-STEM) image of $\text{Ni-N}_3\text{-C}$ clearly display the atomic dispersion of Ni atoms (Figure 1f). The results above clearly confirm the successful construction of single-atom Ni sites in $\text{Ni-N}_3\text{-C}$ after post-synthetic substitution of Zn by Ni atoms.

To further investigate the controlled formation process from $\text{Zn-N}_3\text{-C}$ to $\text{Ni-N}_3\text{-C}$ at atomic scale, the synchrotron-

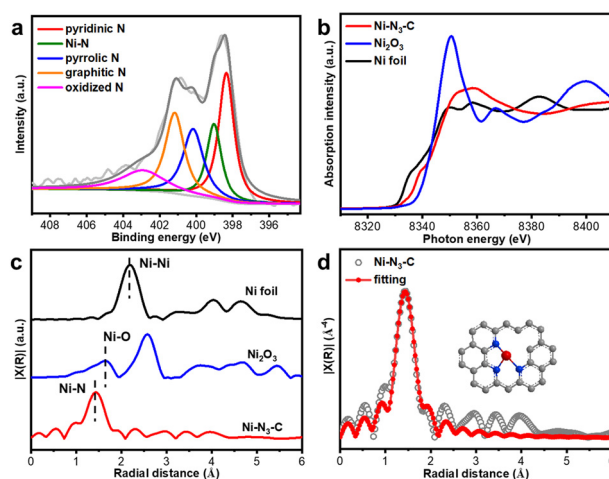


Figure 2. a) The N 1s XPS spectrum of $\text{Ni-N}_3\text{-C}$. b) Ni K-edge XANES spectra and c) FT-EXAFS spectra of $\text{Ni-N}_3\text{-C}$, Ni foil and Ni_2O_3 . d) EXAFS fitting of $\text{Ni-N}_3\text{-C}$ and (inset) optimized coordination environment of Ni atoms.

based X-ray absorption spectroscopy (XAS) measurements have been performed on Zn-N₃-C and Ni-N₃-C. The Zn K-edge X-ray absorption near-edge structure (XANES) spectrum of Zn-N₃-C shows a higher near-edge absorption energy than Zn foil, manifesting that Zn is in an oxidized state in Zn-N₃-C, in line with the XPS results (Figure S9a). In addition, the Zn K-edge Fourier transforms (FT) extended X-ray absorption fine structure (EXAFS) shows the atomic dispersion of Zn atoms without Zn-Zn bonding (Figure S9b). Further EXAFS fitting reveals that each Zn atom is coordinated by 3N atoms, confirming that Zn-N₃ is the dominant coordination mode in Zn-N₃-C (Figure S10, Table S1). After HCl treatment, ≈85% Zn atoms can be removed from Zn-N₃-C, leading to N-C with abundant Zn vacancy (Figure S11). By virtue of the vacancy sites in the N-C, Ni atoms are introduced to afford Ni-N₃-C. As expected, the Ni atoms in the resulting Ni-N₃-C present similar oxidation state and coordination environment to those of Zn in Zn-N₃-C. Specifically, in the Ni K-edge XANES spectrum, the near-edge absorption energy of Ni-N₃-C locates between Ni foil and Ni₂O₃, indicating the oxidized Ni species in Ni-N₃-C (Figure 2b). In addition, the Ni K-edge FT-EXAFS of Ni-N₃-C displays a dominated peak centered at 1.43 Å corresponding to the Ni-N scattering path, and no peaks for Ni-Ni path can be observed (Figure 2c), which clearly suggests the formation of single-atom Ni species. Furthermore, the EXAFS fitting for Ni-N₃-C indicates that each Ni atom is 3-coordinated by three nitrogen atoms, similar to that of Zn in Zn-N₃-C (Figure 2d and S12, Table S2). The high degree of consistency of the oxidation state and coordination number between the single Zn (Zn-N₃-C) and Ni (Ni-N₃-C) atoms perfectly demonstrates the reliability of the PSMS strategy for the rational control of coordination environment.

In light of the characterization results above, the formation process of Ni-N₃-C by PSMS approach can be well understood. Due to the low boiling point (1180 K) of metallic Zn, the generated Zn NPs at high temperature could readily evaporate away in the pyrolysis process of ZIF-8, leaving behind single-atom Zn species coordinated by N atoms in the porous carbon matrix.^[11] Such unique “self-clean” mechanism of Zn element makes it much easier to obtain single-atom Zn at elevated temperature without Zn particles. Meanwhile, the N coordination number of Zn atoms can be finely regulated by controlling pyrolysis temperatures. When the pyrolysis temperature of ZIF-8 reaches 900 °C, the N coordination number of single Zn atoms can be controlled at 3, affording Zn-N₃-C featuring Zn-N₃ sites (Figure S9 and S10). Once the single Zn atoms are removed, abundant Zn vacancies with relatively high energy, which, surrounding by N atoms with lone-pair electrons, are readily occupied by extrinsic metal atoms with empty d orbital by coordination bonding, lowering the energy of the system. In this situation, when Ni atoms are introduced, they are prone to refill into the Zn vacancies spontaneously, thereby producing Ni-N₃-C with abundant Ni-N₃ sites (Figure 2b–d). To further manifest the universality of such PSMS strategy, Zn-N₄-C, with similar physicochemical properties to Zn-N₃-C, has also been constructed at a slightly lower pyrolysis temperature (800 °C), guaranteeing sufficient

N content for the formation of Zn-N₄ sites (Figure S6, S7, S13 and S14, Table S1). Upon acid etching and subsequent Ni decoration, the Ni-N₄-C involving Ni-N₄ sites is constructed (Figure S15, Table S2). To our delight, Ni-N₄-C exhibits similar Ni loading (1.06 wt %) and physicochemical properties to Ni-N₃-C (Figure S5, S6 and S14). Furthermore, Fe-N₃-C and Co-N₃-C, with the central atoms coordinated by 3N atoms, are also successfully fabricated by PSMS process similar to Ni-N₃-C (Figure S16 and S17, Table S3). These results unambiguously manifest the inheritance of both coordination number and microstructure from Zn-N_x-C to Fe-, Co-, and Ni-N_x-C, highlighting the promising universality of PSMS strategy toward the fabrication of SACs with well-controlled coordination number. It can be seen that the core idea of PSMS strategy is the predesign of single-atom Zn catalysts with well-controlled coordination number followed by the exterior metal substitution to inherit the coordination number of single Zn atoms; this provides a new way to the accurate coordination number modulation of SACs.

Encouraged by the results above, electrocatalytic CO₂ reduction over Ni-N_x-C has been examined. As indicated by linear sweep voltammetry (LSV) profiles, Ni-N₃-C presents much larger current response for CO₂ reduction than that of Ni-N₄-C and N-C, suggesting the higher activity of Ni-N₃-C (Figure 3a, S18–S20). Significantly, Ni-N₃-C shows a maximum CO FE up to 95.6% at –0.65 V, far surpassing that of Ni-N₄-C (89.2% at –0.65 V), N-C (76.1% at –0.55 V), Zn-N₃-C (59.5% at –0.60 V) and Zn-N₄-C (56.7% at –0.65 V) (Figure 3b and S21). Meanwhile, the CO FE of Ni-N₃-C can

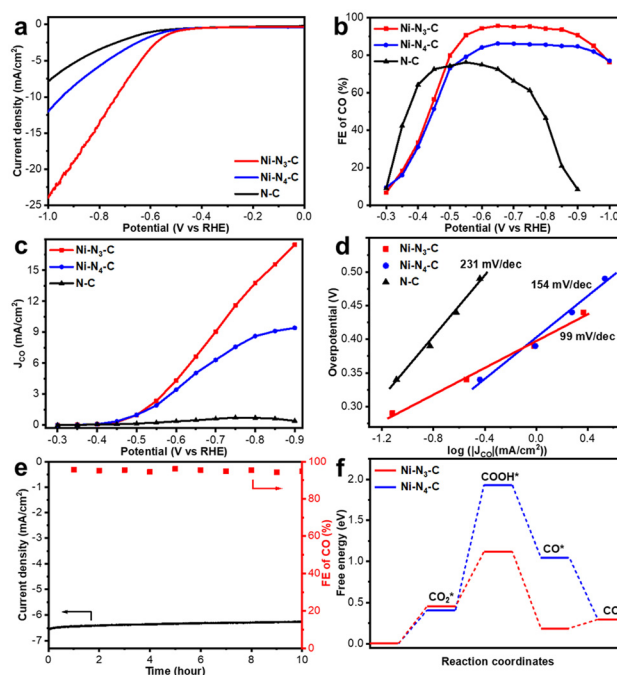


Figure 3. a) LSV curves, b) Faradaic efficiencies, c) CO partial current densities and d) Tafel plots of Ni-N₃-C, Ni-N₄-C and N-C in CO₂-saturated 0.5 M KHCO₃. e) Durability test of Ni-N₃-C at a constant potential of –0.65 V in CO₂-saturated 0.5 M KHCO₃. f) Reaction paths and free energy diagrams of CO₂ reduction to CO for Ni-N₄-C and Ni-N₃-C.

be maintained above 90% in a wide potential window from -0.55 V to -0.9 V with H_2 as the only byproduct (Figure 3b, S22 and S23). Furthermore, Ni-N₃-C shows a CO partial current density (J_{CO}) of 6.64 mA cm⁻² at -0.65 V with a TOF of 1425 h⁻¹, much higher than those of Ni-N₄-C and N-C (Figure 3c and S24). The Tafel slope of Ni-N₃-C is determined to be 99 mV/decade, smaller than that of Ni-N₄-C and N-C, indicating the much favorable kinetics of Ni-N₃-C for CO₂RR (Figure 3d). Meanwhile, Ni-N₃-C also shows smaller charge transfer resistance than Ni-N₄-C, further supporting its much higher catalytic activity (Figure S25). In addition, the best-performed Ni-N₃-C also shows ultrahigh stability with nearly unchanged current density and CO FE under -0.65 V for 10 h (Figure 3e). These results unambiguously manifest that Ni-N₃-C, with lower coordination number of N, exhibits superior catalytic performance for CO₂RR, highlighting the critical role of coordination microenvironment of single-atom Ni sites toward electrocatalysis.

To further understand the excellent performance of Ni-N₃-C for CO₂RR, density functional theory (DFT) calculations have been further conducted (Figure 3f, S26 and S27). Generally, the CO production by CO₂RR is a two-electron and two-proton transfer process in which the formation of COOH* is always the rate-limiting step.^[12] The free-energy change for the formation of COOH* in Ni-N₃-C is determined to be 0.66 eV, far smaller than that of Ni-N₄-C (1.52 eV), displaying the surprisingly lower energy barrier of Ni-N₃-C for CO₂RR, in accordance with the results in above experiments (Figure 3f).

In view of the excellent catalytic performance of Ni-N₃-C toward CO₂RR, the Zn-CO₂ battery, as a promising energy conversion technique for CO₂ utilization,^[13] has been investigated by employing Ni-N₃-C as a cathode catalyst (Figure 4a). In the discharge and charge voltages under different current densities, Ni-N₃-C shows a discharge potential of 0.41 V at 0.5 mA during discharge process (Figure 4b).

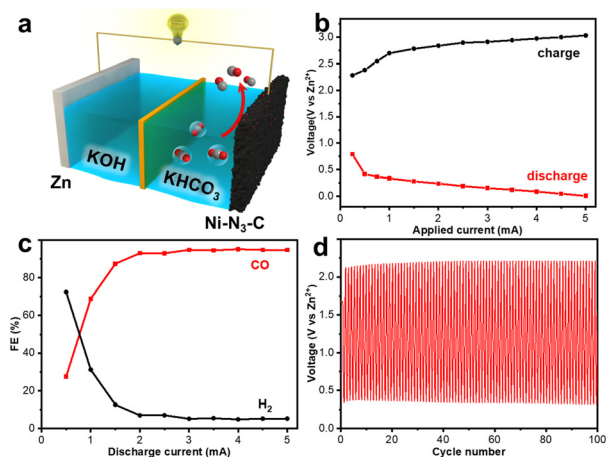


Figure 4. The measurements of Zn-CO₂ battery using Ni-N₃-C as cathode catalyst. a) Schematic illustration for Zn-CO₂ battery. b) Discharge and charge voltage profiles for Zn-CO₂ battery. c) FE of Ni-N₃-C for CO and H₂ during the discharge process under different current densities. d) Galvanostatic discharge-charge cycling curves at 2 mA for 100 cycles.

Encouragingly, when the discharge current reaches 2.5 mA, the discharge potential can be maintained at 0.2 V (Figure 4b). Meanwhile, as an anode in the battery, Ni-N₃-C displays a charge potential of 2.4 V at 0.5 mA, which reaches a relatively stable state after 1 mA (Figure 4b). Moreover, the FE of CO in the discharge process reaches a maximum value of 93% at 2 mA, which can be maintained in a wide discharge current range, manifesting the excellent selectivity to CO of Ni-N₃-C in Zn-CO₂ battery (Figure 4c). In addition, the consecutive discharge-charge cycles at 2 mA present the stable voltage of Ni-N₃-C after 100 cycles, underscoring the excellent durability of the cell (Figure 4d).

In conclusion, a facile and rational PSMS strategy has been developed to fabricate single-atom Ni catalysts by replacing the atomically dispersed Zn sites with Ni atoms in Zn-N_x-C derived from ZIF-8. With this PSMS strategy, the synthesis of SACs from MOF is divided into multi steps yet simplifies the parameters in each step, making the synthesis much more general, controllable and straightforward. Thanks to the unique “self-clean” behavior of the low-boiling metallic Zn during pyrolysis, the single-atom Zn can be readily produced in the absence of concomitant Zn particle. Strikingly, the coordination number of single Zn atoms in Zn-N_x-C can be easily regulated by simply varying the pyrolysis temperature. Once extrinsic Ni atoms are introduced to substitute the single-atom Zn, not only their atomic dispersion but also coordination configuration can be inherited in a well-controlled manner. Remarkably, the optimal Ni-N₃-C, with single-atom Ni coordinated by 3N atoms, displays excellent performance for CO₂ electroreduction with ultrahigh CO FE (95.6%) and TOF value (1425 h⁻¹) at -0.65 V, much higher than those of Ni-N₄-C with Ni-N₄ sites. Theoretical calculations unveil that the lower Ni coordination number in Ni-N₃-C greatly reduces the formation energy of the rate determining step, thereby promoting the CO₂ reduction process. In addition, the assembled Zn-CO₂ battery with Ni-N₃-C as a cathode catalyst offers ultrahigh FE of CO in the discharge process with excellent stability. This work not only demonstrates a facile, novel, general and rationally controlled strategy to manipulate the coordination microenvironment of SACs but also lays a foundation for the promising application of SACs in rechargeable Zn-CO₂ batteries.

Acknowledgements

This work is supported by the NSFC (21725101, 21871244, 21521001, 22001242), China Postdoctoral Science Foundation (2019TQ0298, 2019M660151), International Partnership Program of CAS (211134KYSB20190109), and Collaborative Innovation Program of Hefei Science Center, CAS (2020HSC-CIP005). We acknowledge the XAS supports from BSRF and SSRF. The calculations in this work are supported by the Supercomputing Center of USTC.

Conflict of interest

The authors declare no conflict of interest.

Keywords: CO₂ reduction · coordination environment · electrocatalysis · metal-organic frameworks · single-atom catalysts

- [1] a) A. Wang, J. Li, T. Zhang, *Nat. Rev. Chem.* **2018**, *2*, 65–81; b) Y. Hou, Y.-B. Huang, Y.-L. Liang, G.-L. Chai, J.-D. Yi, T. Zhang, K.-T. Zang, J. Luo, R. Xu, H. Lin, S.-Y. Zhang, H.-M. Wang, R. Cao, *CCS Chem.* **2019**, *1*, 384–395; c) H. Fei, J. Dong, D. Chen, T. Hu, X. Duan, I. Shakir, Y. Huang, X. Duan, *Chem. Soc. Rev.* **2019**, *48*, 5207–5241; d) C. Zhu, S. Fu, Q. Shi, D. Du, Y. Lin, *Angew. Chem. Int. Ed.* **2017**, *56*, 13944–13960; *Angew. Chem.* **2017**, *129*, 14132–14148; e) L. Liu, A. Corma, *Chem. Rev.* **2018**, *118*, 4981–5079; f) C. Zhang, J. M. Tour, *Nat. Catal.* **2018**, *1*, 900–902; g) B. M. Tackett, J. H. Lee, J. G. Chen, *Acc. Chem. Res.* **2020**, *53*, 1535–1544; h) Z. Zhang, J. Sun, F. Wang, L. Dai, *Angew. Chem. Int. Ed.* **2018**, *57*, 9038–9043; *Angew. Chem.* **2018**, *130*, 9176–9181; i) Y. Pan, Y. Qian, X. Zheng, S.-Q. Chu, Y. Yang, C. Ding, X. Wang, S.-H. Yu, H.-L. Jiang, *Natl. Sci. Rev.* **2021**, *8*, nwa224.
- [2] a) P. Liu, N. Zheng, *Natl. Sci. Rev.* **2018**, *5*, 636–638; b) X. Wang, Y. Jia, X. Mao, D. Liu, W. He, J. Li, J. Liu, X. Yan, J. Chen, L. Song, A. Du, X. Yao, *Adv. Mater.* **2020**, *32*, 2000966; c) Y. Zhu, J. Sokolowski, X. Song, Y. He, Y. Mei, G. Wu, *Adv. Energy Mater.* **2020**, *10*, 1902844; d) K. Jiang, S. Back, A. J. Akey, C. Xia, Y. Hu, W. Liang, D. Schaak, E. Stavitski, J. K. Nørskov, S. Siahrostami, H. Wang, *Nat. Commun.* **2019**, *10*, 3997; e) C. Tang, Y. Jiao, B. Shi, J.-N. Liu, Z. Xie, X. Chen, Q. Zhang, S.-Z. Qiao, *Angew. Chem. Int. Ed.* **2020**, *59*, 9171–9176; *Angew. Chem.* **2020**, *132*, 9256–9261; f) X. Li, H. Rong, J. Zhang, D. Wang, Y. Li, *Nano Res.* **2020**, *13*, 1842–1855.
- [3] a) X. Rong, H.-J. Wang, X.-L. Lu, R. Si, T.-B. Lu, *Angew. Chem. Int. Ed.* **2020**, *59*, 1961–1965; *Angew. Chem.* **2020**, *132*, 1977–1981; b) W. Liu, L. Zhang, X. Liu, X. Liu, X. Yang, S. Miao, W. Wang, A. Wang, T. Zhang, *J. Am. Chem. Soc.* **2017**, *139*, 10790–10798; c) F. Li, Y. Bu, G.-F. Han, H.-J. Noh, S.-J. Kim, I. Ahmad, Y. Lu, P. Zhang, H. Y. Jeong, Z. Fu, Q. Zhong, J.-B. Baek, *Nat. Commun.* **2019**, *10*, 2623; d) S. Ji, Y. Chen, X. Wang, Z. Zhang, D. Wang, Y. Li, *Chem. Rev.* **2020**, *120*, 11900–11955; e) L. Jiao, J. Wang, H.-L. Jiang, *Acc. Mater. Res.* **2021**, <https://doi.org/10.1021/accounts.mr.1c00009>.
- [4] a) C. Yan, H. Li, Y. Ye, H. Wu, F. Cai, R. Si, J. Xiao, S. Miao, S. Xie, F. Yang, Y. Li, G. Wang, X. Bao, *Energy Environ. Sci.* **2018**, *11*, 1204–1210; b) A. S. Varela, W. Ju, A. Bagger, P. Franco, J. Rossmeisl, P. Strasser, *ACS Catal.* **2019**, *9*, 7270–7284; c) X. Wang, Z. Chen, X. Zhao, T. Yao, W. Chen, R. You, C. Zhao, G. Wu, J. Wang, W. Huang, J. Yang, X. Hong, S. Wei, Y. Wu, Y. Li, *Angew. Chem. Int. Ed.* **2018**, *57*, 1944–1948; *Angew. Chem.* **2018**, *130*, 1962–1966.
- [5] a) Y. Pan, Y. Chen, K. Wu, Z. Chen, S. Liu, X. Cao, W.-C. Cheong, T. Meng, J. Luo, L. Zheng, C. Liu, D. Wang, Q. Peng, J. Li, C. Chen, *Nat. Commun.* **2019**, *10*, 4290; b) L. Jiao, H.-L. Jiang, *Chem* **2019**, *5*, 786–804.
- [6] a) H.-C. Zhou, J. R. Long, O. M. Yaghi, *Chem. Rev.* **2012**, *112*, 673–674; b) T. Islamoglu, S. Goswami, Z. Li, A. J. Howarth, O. K. Farha, J. T. Hupp, *Acc. Chem. Res.* **2017**, *50*, 805–813; c) H. Li, L. Li, R.-B. Lin, W. Zhou, Z. Zhang, S. Xiang, B. Chen, *EnergyChem* **2019**, *1*, 100006; d) Y.-Z. Chen, R. Zhang, L. Jiao, H.-L. Jiang, *Coord. Chem. Rev.* **2018**, *362*, 1–23.
- [7] a) Y.-S. Wei, M. Zhang, R. Zou, Q. Xu, *Chem. Rev.* **2020**, *120*, 12089–12174; b) T. Qiu, Z. Liang, W. Guo, T. Hassina, S. Gao, R. Zou, *ACS Energy Lett.* **2020**, *5*, 520–532; c) L. Jiao, R. Zhang, G. Wan, W. Yang, X. Wan, H. Zhou, J. Shui, S.-H. Yu, H.-L. Jiang, *Nat. Commun.* **2020**, *11*, 2831; d) H. Yang, Q. Lin, C. Zhang, X. Yu, Z. Cheng, G. Li, Q. Hu, X. Ren, Q. Zhang, J. Liu, C. He, *Nat. Commun.* **2020**, *11*, 593.
- [8] a) A. Guan, Z. Chen, Y. Quan, C. Peng, Z. Wang, T.-K. Sham, C. Yang, Y. Ji, L. Qian, X. Xu, G. Zheng, *ACS Energy Lett.* **2020**, *5*, 1044–1053; b) X. Li, L. Liu, X. Ren, J. Gao, Y. Huang, B. Liu, *Sci. Adv.* **2020**, *6*, eabb6833; c) T. Sun, L. Xu, D. Wang, Y. Li, *Nano Res.* **2019**, *12*, 2067–2080.
- [9] a) X.-C. Huang, Y.-Y. Lin, J.-P. Zhang, X.-M. Chen, *Angew. Chem. Int. Ed.* **2006**, *45*, 1557–1559; *Angew. Chem.* **2006**, *118*, 1587–1589; b) K. S. Park, Z. Ni, A. P. Côté, J. Y. Choi, R. Huang, F. J. Uribe-Romo, H. K. Chae, M. O’Keeffe, O. M. Yaghi, *Proc. Natl. Acad. Sci. USA* **2006**, *103*, 10186–10191.
- [10] L. Jiao, W. Yang, G. Wan, R. Zhang, X. Zheng, H. Zhou, S.-H. Yu, H.-L. Jiang, *Angew. Chem. Int. Ed.* **2020**, *59*, 20589–20595; *Angew. Chem.* **2020**, *132*, 20770–20776.
- [11] a) J. Li, S. Chen, N. Yang, M. Deng, S. Ibraheem, J. Deng, J. Li, L. Li, Z. Wei, *Angew. Chem. Int. Ed.* **2019**, *58*, 7035–7039; *Angew. Chem.* **2019**, *131*, 7109–7113; b) Q. Yang, C.-C. Yang, C.-H. Lin, H.-L. Jiang, *Angew. Chem. Int. Ed.* **2019**, *58*, 3511–3515; *Angew. Chem.* **2019**, *131*, 3549–3553.
- [12] a) H.-J. Zhu, M. Lu, Y.-R. Wang, S.-J. Yao, M. Zhang, Y.-H. Kan, J. Liu, Y. Chen, S.-L. Li, Y.-Q. Lan, *Nat. Commun.* **2020**, *11*, 497; b) C. He, Y. Zhang, Y. Zhang, L. Zhao, L.-P. Yuan, J. Zhang, J. Ma, J.-S. Hu, *Angew. Chem. Int. Ed.* **2020**, *59*, 4914–4919; *Angew. Chem.* **2020**, *132*, 4944–4949; c) M. Liu, Y. Pang, B. Zhang, P. D. Luna, O. Voznyy, J. Xu, X. Zheng, C. T. Dinh, F. Fan, C. Cao, F. P. García de Arquer, T. S. Safaei, A. Mepham, A. Klinkova, E. Kumacheva, T. Filleter, D. Sinton, S. O. Kelley, E. H. Sargent, *Nature* **2016**, *537*, 382–386; d) F. Lv, N. Han, Y. Qiu, X. Liu, J. Luo, Y. Li, *Coord. Chem. Rev.* **2020**, *422*, 213435.
- [13] J. Xie, Y. Wang, *Acc. Chem. Res.* **2019**, *52*, 1721–1729.

Manuscript received: December 6, 2020

Accepted manuscript online: January 11, 2021

Version of record online: February 26, 2021